Scientific paper

Evaluating SAXS Results on Aqueous Solutions of Various Bacterial Levan utilizing the String-of-Beads Model

Elizabeta Benigar,[1] Matija Tomšič,[1] Simon Sretenovic,[2] David Stopar,[2] Andrej Jamnik[1] and Iztok Dogsa[2]*

[1] *University of Ljubljana, Faculty of Chemistry and Chemical Technology, Večna pot 113, SI-1000 Ljubljana, Slovenia*

2 University of Ljubljana, Biotechnical Faculty, Večna pot 111, SI-1000 Ljubljana, Slovenia

** Corresponding author: E-mail: Iztok.Dogsa@bf.uni-lj.si*
Tel: +386 1 320 3414

Received: 17-02-2015

Dedicated to prof. Jože Koller on the occasion of his 70th birthday.

Abstract

Polysaccharide levan is a homopolymer of fructose and is an important component of plants, yeast, fungi and some bacterial biofilms. In this paper we report on the structural properties of aqueous solutions of bacterial levan utilizing small-angle X-ray scattering and light microscopy. In addition to commercially available levan isolated from *Zymomonas mobilis* and *Erwinia herbicola*, we also studied levan isolated and purified from the biofilm of *Bacillus subtilis*. The small-angle X-ray scattering data were analyzed by the string-of-beads model that revealed qualitative differences in the structure of levan molecules. Levan can be represented as a semi-flexible chain that interacts intra- and inter-molecularly and therefore forms various suprastructures on larger size scales. Increasing the concentration of levan makes the levan structure more compact, which was observed on the nano as well as on the micro scale. The structures with most homogeneously distributed polymer local density were found in *B. subtilis* levan solutions.

Keywords: Levan, *Bacillus subtilis*, *Erwinia herbicola*, *Zymomonas mobilis*, SAXS, string-of-beads model

1. Introduction

Levan is a water soluble polysaccharide composed of fructofuranosyl rings, connected by β-(2,6) glycosidic linkages and occasional branching through β-(2,1) glycosidic linkages. Levan of bacterial origin typically contains from 9 to 12% of such branching points.[1–5] Structure of levan is stable from pH 4 to pH 11, at concentrations of inorganic salts from 20 to 30% and temperatures up to 70 °C.[6] Levan is widespread – it is found in plants, yeast, fungi and bacterial biofilms.[7] Biofilms are multicellular microbial communities embedded in extracellular polymeric matrix (EPS-matrix) and levan can represent a major polymer component, as for example in *B. subtilis* subs. *subtilis* strain NCIB 3610 biofilms, grown in a sucrose rich liquid medium.[5,8] Biofilms based on levan can play a key role in the development of plant diseases,[9] dental caries and periodontal disease.[10,11] Levan shows extremely low intrinsic viscosity and exhibits a rather atypical non-gelling behavior in aqueous solutions in comparison to most other common polysaccharides.[3,12] At high concentrations of up to 8 wt % levan can nevertheless support rather robust biofilms.[12] Levan from *Bacillus* sp. behaves like a newtonian fluid up to 30 wt % solution and is soluble even up to 60 wt % solution.[3,13] Modelling attempts to resolve the structural details of such polysaccharide systems based on small-angle X-ray scattering (SAXS) results are very scarce.[5,14]

In the present study we focus on the detailed interpretation of SAXS data obtained for 1, 2, 4, 6, and 8 wt % aqueous levan solutions of three bacteria: *Bacillus subtilis (BS), Zymomonas mobilis (ZM) and Erwinia herbicola (EH)*. In our previous structural and rheological study we have shown that the mole fraction of branching

points was (10.5 ± 0.7) % in *B. subtilis* levan, (11.0 ± 0.7) % in *Z. mobilis* levan, and (10.2 ± 0.3) % in *E. herbicola* levan. The intrinsic viscosity value for *B. subtilis* levan was (0.35 ± 0.04) dL/g, for *Z. mobilis* levan (0.36 ± 0.01) dL/g, and for *E. herbicola* levan (0.45 ± 0.01) dL/g. The hydration number for all three samples was around 6. Levan samples also showed very similar viscosities at low concentrations (1 wt %), while viscosities varied significantly at higher concentrations. In concentration range from 1 to 8 wt % all three samples showed elastic character. Another difference between studied levan samples was in the weight average molecular weight M_w. The estimate for M_w of *B. subtilis* levan was (31 ± 2) MDa, of *Z. mobilis* levan (226 ± 4) MDa, and of *E. herbicola* levan (280 ± 40) MDa. These results were consistent with the ones obtained by light microscopy. The largest particles of (0.5 ± 0.3) μm were observed in *E. herbicola* levan solution, followed by *Z. mobilis* levan particles of (0.45 ± 0.10) μm and *B. subtilis* levan particles of (0.35 ± 0.10) μm in diameter in 1 % (w/v) aqueous solutions. The SAXS data of different levans were analyzed and interpreted by the classical approach utilizing the Ornstein-Zernike[15,16] and an additional Debye-Bueche[16–18] term.[5] Unfortunately the classical approach failed to provide the information on the static correlation length, i.e. we could not satisfactorily describe the SAXS intensities in the innermost regime of the scattering curves.[5] Therefore, in this work, we applied a more complex string-of-beads model[20–21] to describe experimental SAXS curves, and propose a new levan supramolecular structure in the aqueous solution.

2. Experimental and Methods

2. 1. Materials

In this study three different samples of bacterial levan were used. Two of them were commercially available levans isolated from *Z. mobilis* (Sigma Aldrich) and *E. herbicola* (Sigma Aldrich). The third sample was obtained from biofilm of *B. subtilis* subs. *subtilis* strain NCIB 3610. Detailed isolation and purification procedures are described by Dogsa et al. (2013)[8] and Benigar et al. (2014).[5] The purity of isolated *B. subtilis* levan (98.3%) was comparable to purity of commercial levans isolated from *E. herbicola* (98.5%) and *Z. mobilis* (98.8%).[5] Levan samples for SAXS measurements were prepared as 1, 2, 4, 6, and 8 wt % aqueous solutions utilizing strong vortex mixing. Levans originating from bacteria *B. subtilis*, *Z. mobilis* and *E. herbicola* are hereinafter referred to as BS, ZM and EH levans, respectively.

2. 2. Light Microscopy

The microscopy was performed with an Axio Observer Z1 inverted microscope (Zeiss, Gottingen, Germany) equipped with Zeiss Plan-Apochromat 100x/1.40 Oil immersion objective and MRm AxioCam camera using the differential interference contrast technique (DIC). The magnification was further enhanced by using 2.5 fold internal lens (optovar). For slide preparation 5 μL of sample was spotted on a clean glass slide and covered with a cover glass with a thickness of #1.5. The prevention of water evaporation from the sample on the slide was accomplished by sealing the gap between the slide and the cover glass. For flat-field correction the out-of-focus images, where uneven light distribution can be observed, were taken for each sample. The images were processed by Imagej software (ver. 1.48b, W. Rasband, NIH, USA). Firstly, by normalizing sample image on out-of-focus image the flat-field correction was achieved. Then the enhance contrast function of imageJ was applied. The particles were manually measured by drawing straight lines over them representing their diameter. In this way at least 50 levan particles were analysed. In order to exclude the biased selection of the levan particles the horizontal and vertical lines across the full-size of the processed image were drawn and only levan particles on the lines were considered.

2. 3. Small-Angle X-Ray Scattering Measurements

Levan samples were measured at 25 °C with a Kratky compact camera (Anton Paar KG, Graz, Austria). The camera was attached to a conventional X-ray generator (Kristalloflex 760, Bruker SAXS GmbH, Karlsruhe, Germany) equipped with a sealed X-ray tube (Cu K_α X-rays, $\lambda = 0.154$ nm) operating at 40 kV and 35 mA. Monochromatic primary beam was attenuated by a Ni foil of appropriate thickness due to the limitations of the detector. In addition a software monochromator was used to register only the scattered X-ray photons within a predefined range of energies. The samples were measured in a standard quartz capillary with an outer diameter of 1 mm and wall thickness of 10 μm. The scattered X-ray intensities were detected with a PSD-50M ASA position sensitive detector (M. Braun GmbH, Garching, Germany) in the small-angle regime of scattering vectors given by ($0.07 < q < 7$) nm^{-1}, where $q = 4\pi/\lambda \cdot \sin(\vartheta/2)$. Each individual sample was measured for 24 to 48 hours to yield reliable measurement statistics. Prior to further analysis the scattering data were corrected for the empty capillary and pure solvent scattering, and normalized to an absolute scale using water as a secondary standard.

2. 4. Interpretation of SAXS Data – »String-of-Beads« Model

For the interpretation of SAXS curves the string-of-beads model developed by Dogsa et al.[19–21] was applied. In this model the polymer or the polymer segment is si-

mulated as a linear chain of sequential spherical beads approximating monomers. The validity of this approximation was verified in our previous paper,[21] where we calculated the theoretical scattering curves of sugar trimers at atomic level and compare them to the theoretical scattering curves of superimposed structures made of three beads. In the case of levan, which is uncharged β–fructan, a basic monomer unit is fructose. The position of the bead in the polymer molecule, relative to its predecessor, is described by Θ (bond) and Φ (torsion) angles. Each pair of angles is set according to the probability p^* (Θ_p and Φ_p) for the random variation of the angles Θ and Φ between adjacent beads. For example, if $p^* = 0$ the polymer forms a rigid helical structure. If $p^* = 1$ all monomers have random Θ and Φ values and this translates to a random conformation of the polymer molecule (chain). To further vary the stiffness of a polymer chain an additional parameter, Θ_{plim}, is used. This parameter sets the upper limit of the bond angle Θ in the simulation. In addition, one can also vary the size of the polymer chain N, i.e. the number of monomers per chain. For this study the chains with N ranging from 25 to 1000 monomers were modeled.

The algorithm firstly calculates the representative form factor, $\overline{P(q)}$, of the modeled chain with size ξ_S (= $2R_g$), shown in Figure 1, for each set of the four shape parameters.[20,21] Each representative form factor is combined with the term representing the intermolecular interactions into a total scattering function $I(q)$ according to the following expression:[20]

$$I(q) = \Delta\rho^2 \left[\frac{8\pi \langle \delta\varphi^2 \rangle \Xi^3}{(1+q^2\Xi^2)^2} + \frac{\langle \varphi \rangle v_0}{1+Ke^{-q^2\xi^2}} \overline{P(q)} \right], \qquad (1)$$

where $\Delta\rho^2$ is the scattering length density difference between polymer and solvent, $\langle \delta\varphi^2 \rangle$ is variance of the volume fraction of the polymer, $\langle \varphi \rangle$ is the mean volume fraction of the polymer, v_0 is the single polymer chain or polymer segment volume, K is the constant proportional to the strength of the repulsive interactions, ξ is the correlation length over which the repulsion occurs, q is scattering vector, Ξ is correlation length that describes the average size of the Debye inhomogeneities (Figure 1),[24] which cause fluctuations in the local volume fraction of the polymer. Model equation is then fitted to the experimental SAXS data and only solutions with sufficiently good fits are taken into further consideration.[20] While fitting, only one type of interaction is assumed to be presented in the system, i.e. either $\langle \delta\varphi^2 \rangle > 0$ and $K = 0$ or $\langle \delta\varphi^2 \rangle = 0$ and $K > 0$. Based on solutions of interaction parameters one can than simulate the suprastructure made of individual polymer chains or polymer segments.[20] The volume fraction of the polymer is assumed to be log-normally distributed through space.[20,25]

In the present study we apply this modelling approach on semi-concentrated aqueous solutions of various

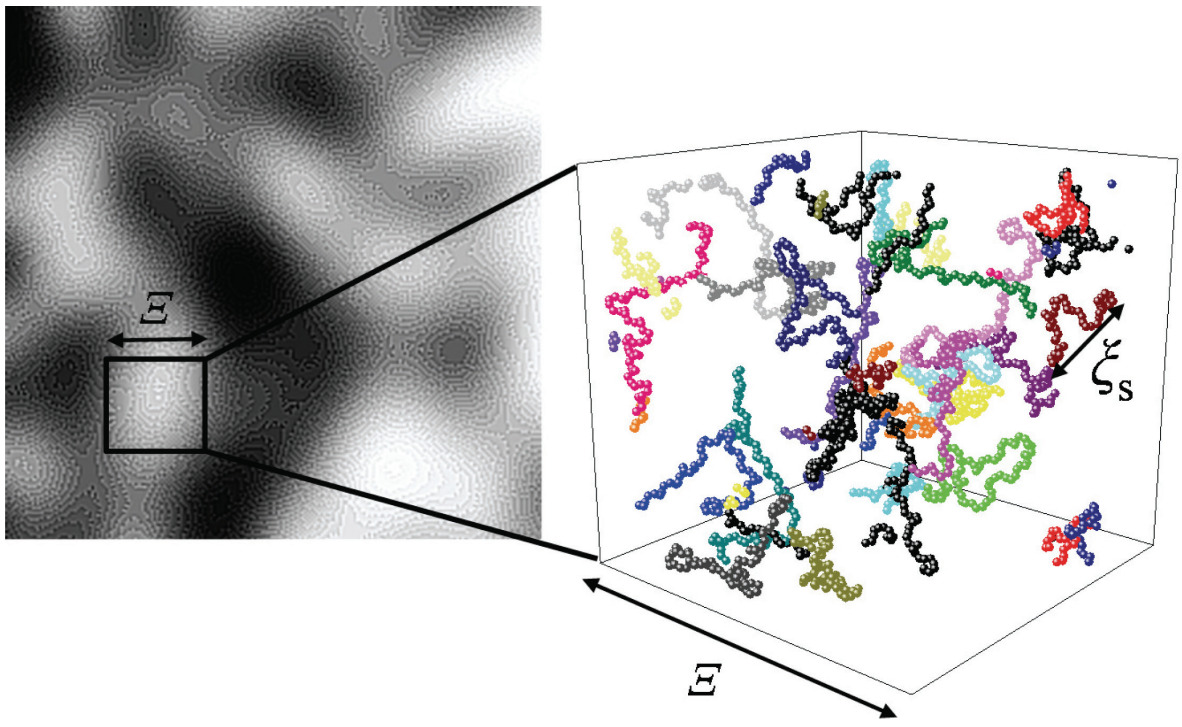

Figure 1: Scheme illustrating two correlation length parameters occurring in levan samples: Ξ describes the average size of the Debye inhomogeneities, while ξ_S (= $2R_g$) represents the size of the simulated polymer segment. Each segment is represented in different color. Ξ on the scheme corresponds to 300 Å. The contours on the left-hand side scheme indicate the regions with the same local polymer density (i.e. volume fraction of the polymer). White color represents high density, black low density.

samples of aggregating non-ionic polysaccharide levan obtained from different bacterial origins.

3. Results and Discussion

3. 1. Small-Angle X-ray Scattering and Modelling Results

When applying the SAXS technique one has to be aware that due to the limited range of the scattering vector available by this technique, structural details from approximately 1 nm up to a few tens of nm can be obtained. This means that in the studies of the polymer systems SAXS technique can successfully reveal the structural information on the molecular level, whereas for the information on the macroscopic structure usually other methods need to be applied. In combination with an appropriate molecular model one can usually obtain geometrical parameters of the macromolecules in solution. SAXS technique has previously been successfully applied in the structural studies of various polysaccharides,[5,19–21,26–28] while SAXS studies on polysaccharide levan are scarce.[5,14] In the present study we apply the string-of-beads model according to eq. (1) to the experimental SAXS scattering data of 1, 2, 4, 6, and 8 wt % BS, ZM, and EH levan samples. Since levan is an uncharged polymer, the parameter K, describing the strength of repulsive interaction was set to 0. Experimental SAXS data of 1, 2, and 8 wt % BS, ZM, and EH levan samples are shown in a double logarithmic plot in Figure 2. The symbols represent the experimental data and the full lines correspond to the best fits obtained by the string-of-beads model. As can be seen from the scattering curves the BS levan most notably differs from the other two levan samples. Such a relationship was observed also in the case of macroscopic rheological, sound velocity and hydration results, which suggests that the molecular and macroscopic structures are in levan strongly related.

The result of string-of-beads model is a set of all solutions satisfying the fit quality criteria[20] each of which comprises the values of the interaction parameters and the corresponding set of four shape parameters: Θ_p, Φ_p, Θ_{plim}, and p^*. The ranges of resulting parameters for levan samples are given in Table 1a and b. In addition, the 3D representation of the polymer structure parameters obtained from the best fits of 2 wt % levan are depicted in Figure 3. The cube contains points corresponding to all good fit solutions. A representative molecular structure of the polymer segment is depicted below the cube. It can be observed that none of the structures represents a true random coil as p^*-values are much smaller than 1. In general, levans adopt semi-flexible chain conformations irrespective of concentration with p^* between 0.1–0.7. However, the p^*-values of BS are higher than p^*-values of ZM or EH, which means that the BS modeled chains in comparison to ZM or EH adopt conformations that are more similar to those characteristic for random coil. At the same time other shape parameters (Θ_p, Φ_p, Θ_{plim}) do not vary significantly. Therefore the chain segments of BS levan structure are more flexible than the segments of ZM or EH levan, which is in agreement with the previous observation that BS levan had the lowest viscosity.[5] This is a characteristic of

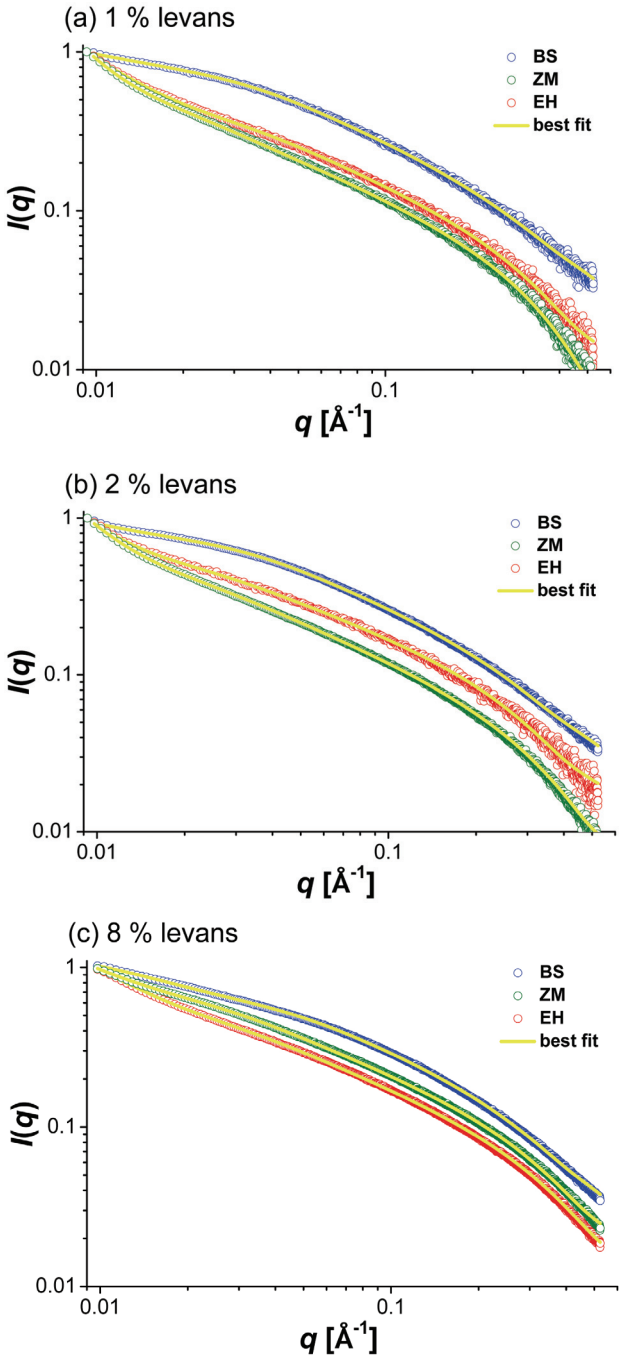

Figure 2: Log-log plots of experimental SAXS curves (open symbols) of (a) 1 wt % BS (○), ZM (○), and EH (○) levan, (b) 2 wt % BS (○), ZM (○), and EH (○) levan, and (c) 8 wt % BS (○), ZM (○), and EH (○) levan. The solid lines represent best fits to the data by the string-of-beads model according to eq.

polymers with small persistence length,[29] typically occurring in random coils. At this point we have to comment on the values of the parameter *N* in Table 1, which represents the number of beads in the string. The value of *N* does not represent the whole levan molecule (individual polymer), but rather its shorter entangled segments (Figure 1).

It is important to point that not all of the values of parameter *N* provide good fits – if the value was too large or too low no satisfactory fitting solution was obtained. The lowest values of parameter *N*, as well as ξ_S were obtained for BS levan. Because the electrostatic interaction is not present in uncharged levan ($K = 0$), the second term in eq. 1 assumes that modeled segments are randomly distributed in space. Therefore the size of the segment, ξ_S (Figure 1) is also the distance above which the individual segments become uncorrelated in space. This means that BS structure is not only the most random at the level of the individual chain segment, but also at the level of segment arrangements. This is in the agreement with our previous DLS (dynamic light scattering) results, where the relaxation times were the fastest in BS levan.[5] Increasing the levan concentration, decreases the segment size *N*, as well as segment ξ_S. This can be explained by the observation that in these levan samples critical overlap concentration is reached for concentrations above 1 wt %,[5] which forces the levan molecules to adopt more dense structure. Because segments build suprastructures, one expects that segments will impact the behavior on the larger size scale. The correlation length of Debye-Bueche heterogeneities Ξ is lowest in BS levan and decreases with levan concentration in all levans. Supramolecular structures of 2 wt % BS, ZM, and EH levan are shown in Figure 4 and were simulated based on the log-normal distributions of levan polymer density (i.e. volume fraction of the polymer), which was obtained from $\langle\delta\varphi^2\rangle/\langle\varphi\rangle^2$ and $\langle\varphi\rangle$. For example, subspaces $\varphi_{5\%}$ indicate the characteristic subspace levan distribution, which is found in 5% of the levan sample volume. The local polymer density in the high density ex-

Table 1. a) Interaction parameters of the fits to the experimental SAXS data, and b) shape parameters for BS, ZM, and EH levans. The ranges of parameter values of good fits are given:

a) Interaction fitting and calculated parameters					
w_{levan} **[wt. %]**	**1**	**2**	**4**	**6**	**8**
BS					
N	75	75	50	40	40
$\langle\delta\varphi^2\rangle/\langle\varphi\rangle^2$	0.26–0.94	0.14–0.16	0.12–0.17	0.17–0.23	0.10–0.15
Ξ [Å]	71–180	120–150	60–75	55–65	65–70
ξ_S [Å]	68–86	78–82	58–62	50–54	55
EH					
N	50–200	100	100	75	75
b) Model shape parameters					
w_{levan} **[wt. %]**	**1**	**2**	**4**	**6**	**8**
Ξ [Å]	90–890	320–450	240–260	120–240	100–125
ξ_S [Å]	60–140	100–101	98–100	68–82	78–85
ZM					
N	150–200	150	100	100	50–75
$\langle\delta\varphi^2\rangle/\langle\varphi\rangle^2$	2.2–10	1.5–1.6	0.97–1.00	0.30–0.32	0.14–0.20
Ξ [Å]	170–1300	270–290	170–190	150–180	90–180
ξ_S [Å]	98–140	110	95–100	95–110	81–102
BS					
θ_{plim}	1.25–2.0	1.5–2.0	1.25–2.0	1.5–2.0	1.65–1.85
θ_p	0.0–1.9	0.7–1.1	0.7–1.4	0.5–1.3	0.9–1.1
Φ_p	0.2–3.1	1.0–2.1	1.3–3.0	1.3–3.1	1.3–1.5
p^*	0.25–0.75	0.3–0.55	0.35–0.7	0.35–0.70	0.325–0.375
EH					
θ_{plim}	1.25–2.0	1.75–2.0	1.75–1.9	1.5–2.0	1.4–2.0
θ_p	0.8–1.9	1.05–1.10	1.15–1.2	1.1–1.9	1.15–1.45
Φ_p	0.9–3.1	1.24–1.29	1.4–1.5	1.4–2.6	1.4–1.75
p^*	0.1–0.6	0.22–0.25	0.25–0.275	0.30–0.45	0.275–0.35
ZM					
θ_{plim}	1.25–2.0	1.9–2.0	1.6–2.0	1.4–2.0	1.4–2.0
θ_p	1.2–1.9	1.1–1.4	1.1–1.35	1.15–1.35	1.15–1.35
Φ_p	1.0–1.6	1.2–1.4	1.4–1.75	1.45–1.65	1.5–1.85
p^*	0.15–0.25	0.225–0.275	0.275–0.325	0.275–0.35	0.275–0.375

treme is much higher in ZM and EH levan than in BS levan. On the other hand, in the low density extreme the local polymer density of BS levan is higher compared to the other two levans. Furthermore, BS levan molecules were the most homogeneously distributed, as the variations among subspaces were the smallest. ZM and EH levans had virtually identical density distribution. This is in agreement with calculated relative fluctuation of volume fraction of the polymer $\langle\delta\varphi^2\rangle/\langle\varphi\rangle^2$ (Table 1a), which measures the heterogeneity of the system on the size scale of Ξ. It is lowest in BS and decreases with concentration in all levans.

As the molecular suprastructures build macrostructures the behavior of levan was also studied under the microscope.

3. 2. Microscopy Results

To complement the interpretation of SAXS data light microscopy was used. As shown already in our previous study[5] 1% (w/v) BS, ZM, and EH levans in aqueous solution form spherical particles. In the present study we used the differential interference contrast microscopy (DIC) to investigate an extended range of aqueous solutions of 1, 2, 4, and 6% (w/v) BS, ZM, and EH levan. We also prepared 8% (w/v) levan solutions, but ZM and EH levan samples were too dense to observe individual levan particles. The microscopy images of 1 and 6% (w/v) levan solutions are depicted in Figure 5. As can be observed the number of BS levan particles was much smaller than the number of ZM and EH levan particles. The levan particles became smaller and more homogeneously distributed with increasing concentration. The effect was most noticeable in EH levan solutions and the least in BS levan solutions. Average sizes of BS, ZM, and EH levan particles are presented in Table 2. The average size of 1% (w/v) ZM and EH levan particles was similar, while the average size of 1% (w/v) BS levan particles was significantly smaller. Similar trend can be also observed for 2% (w/v) levans. This is in accordance with the observations that levans of BS have the highest p*-values and lowest number of monomers per segment, *N*, as obtained from SAXS (Table 1). Such segments have small radius of gyration and are more flexible. Therefore one could expect that superposing these segments results in smaller structures, which was indeed observed. However, with increasing concentration the difference in size between the three levan particles decreased and finally the average size of 6% (w/v) BS, ZM, and EH levan particles were comparable (Table 2). This agrees with our observation that with increasing concentration levan molecules become more compact on nanoscale.

Table 2. Average diameter of BS, EH, and ZM levan particles at 1, 2, 4, and 6 % (w/v) concentrations. Error estimate for average diameter is ± 0.10 μm.

	Average diameter *d* [μm]		
γ [%, (w/v)]	**BS**	**EH**	**ZM**
1	0.45	0.65	0.65
2	0.40	0.60	0.55
4	0.40	0.45	0.50
6	0.35	0.35	0.45

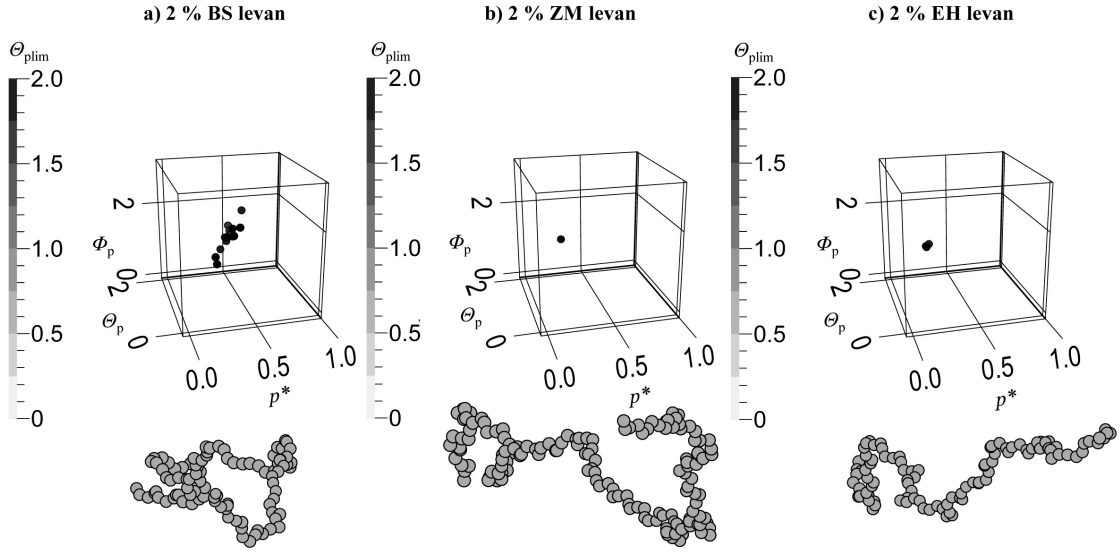

Figure 3. Graphical presentation of the results of the string-of-beads model obtained for the experimental scattering curves shown in Figure 2b. Below: Best-fit conformations for: a) 2 wt % BS levan (Θ_{plim} = 1.75, Θ_p = 0.9, Φ_p = 1.241, and p^* = 0.35), b) 2 wt % ZM levan (Θ_{plim} = 2, Θ_p = 1.3, Φ_p = 1.296, and p^* = 0.25) and c) 2 wt % EH levan (Θ_{plim} = 2, Θ_p = 1.05, Φ_p = 1.246, and p^* = 0.225). Above: Resulting shape parameters are presented as grayscale points in 3D cubes.

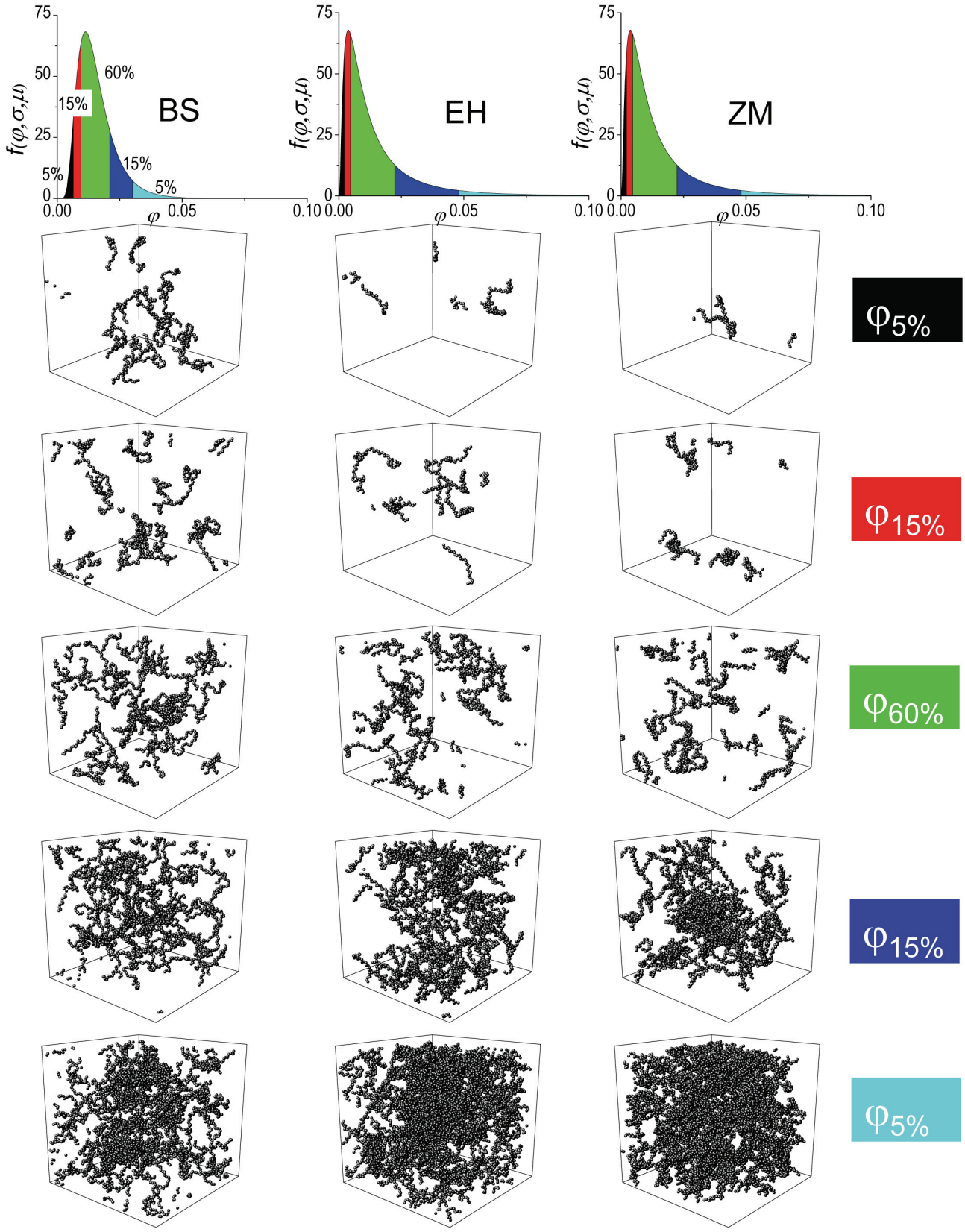

Figure 4. Molecular distribution of 2 wt % levan in space, calculated from interaction parameters presented in Table 1 and the best-fit shape parameters from Figure 3. On the right-hand side of the figure index of φ represents the probability to encounter a characteristic subspace with the local φ in a levan sample. Assumptions: $\rho(H_2O) = 9.47 \times 10^{-6}$ cm^{-2}, ρ(levan) = 1.31×10^{-5} cm^{-2}, levan mass density = 1.45 g/cm^3. The size of the monomer bead (5.2 Å) is depicted in proportion to the side-length of the subspace box (300 Å).

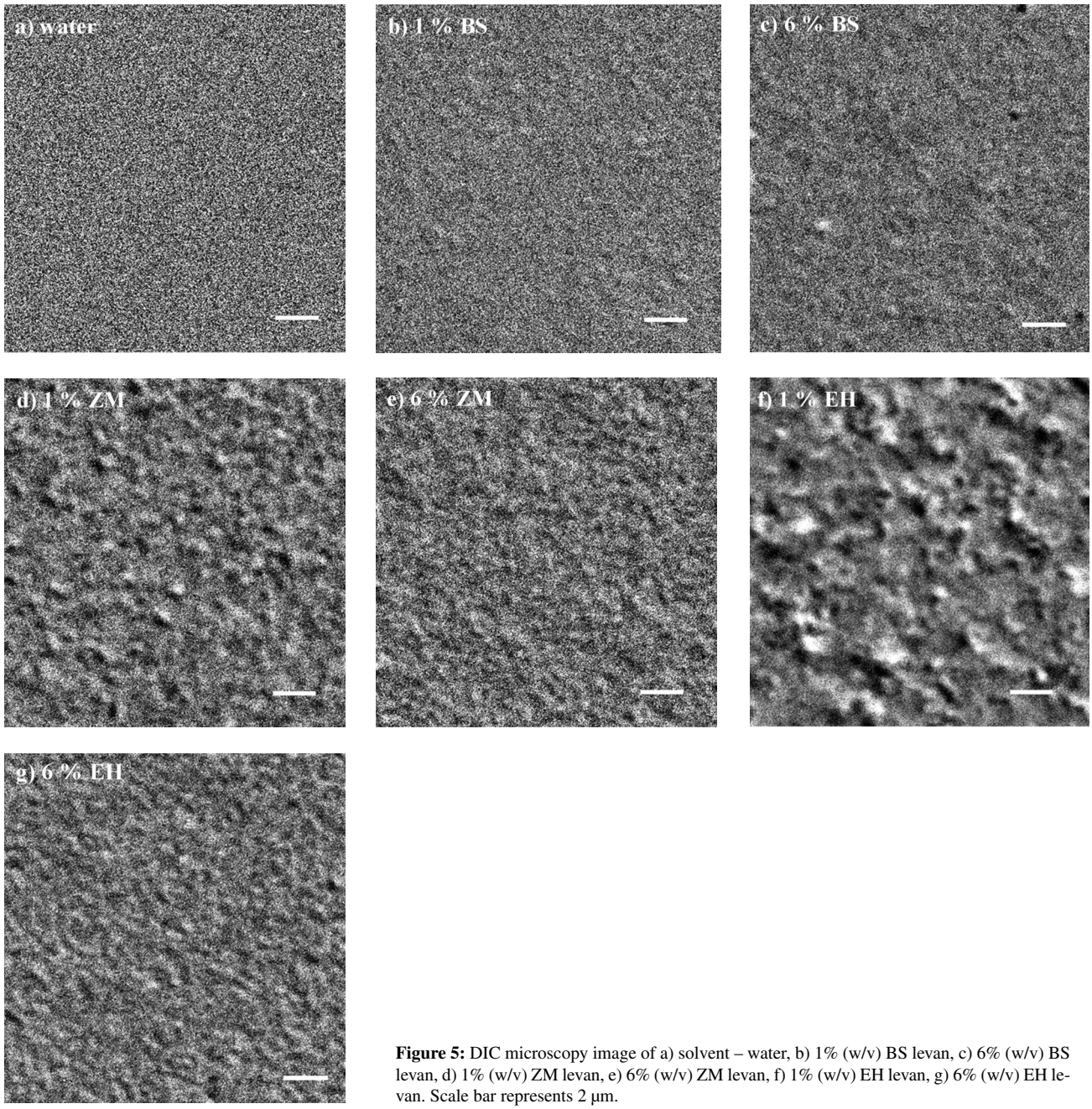

Figure 5: DIC microscopy image of a) solvent – water, b) 1% (w/v) BS levan, c) 6% (w/v) BS levan, d) 1% (w/v) ZM levan, e) 6% (w/v) ZM levan, f) 1% (w/v) EH levan, g) 6% (w/v) EH levan. Scale bar represents 2 μm.

4. Conclusions

Structural properties of different bacterial levan aqueous solutions were studied with SAXS technique. The results of modelling SAXS curves indicate that with increasing concentration levan molecules in aqueous solution become more compact. This phenomenon propagates from nanoscale to microscale of levan. Heterogeneity of the levan suprastructure decreases with increasing levan concentration. The most random and homogeneously distributed structures can be found in BS levan aqueous solutions.

5. Acknowledgment

We are grateful to prof. Otto Glatter for his generous contribution to the instrumentation of our laboratory for the light scattering methods. We are also thankful to Slovenian Research Agency for their financial support (programs P1-0201 and P4-0116).

6. References

1. D. J. Bell, R. Dedonder, *Journal of the Chemical Society*

1954, 2866–2870.
2. E. Newbrun, R. Lacy, T. M. Christie, *Archives of Oral Biology* **1971**, *16*, 863–872.
3. Y. W. Han, M. A. Clarke, *J. Agric. Food Chem.* **1990**, *38*, 393–396.
4. D. Rolf, G. R. Gray, *Carbohydr. Res.* **1984**, *131*, 17–28.
5. E. Benigar, I. Dogsa, D. Stopar, A. Jamnik, I. Kralj Cigicì, M. Toms¡ič, *Langmuir* **2014**, *30*, 4172–4182.
6. I. Vina, A. Karsakevich, S. Gonta, R. Linde, M. Bekers, *Acta Biotechnol.* **1998**, *18*, 167–174.
7. Y. W. Han, *Adv. Appl. Microbiol.* **1990**, *38*, 171–194.
8. I. Dogsa, M. Brloznik, D. Stopar, I. Mandic-Mulec, *PLoS One* **2013**, *8*, e62044.
9. J. M. Koczan, M. J. McGrath, Y. Zhao, G. W. Sundin, *Phytopathology* **2009**, *99*, 1237–1244.
10. H. Mukasa, D. H. Slade, *Infect. Immun.* **1974**, *10*, 1135–1145.
11. R. S. Manly, D. T. Richardson, *J. Dent. Res.* **1968**, *47*, 1080–1086.
12. S. A. Arvidson, B. T. Rinehart, F. Gadala-Maria, *Carbohydr. Polym.* **2006**, *65*, 144–149.
13. S. A. Arvidson, B. T. Rinehart, F. Gadala-Maria, *Carb. Polym.* **2006**, *65*, 144–149.
14. B. A. Khorramian, S. S. Stivala, *Carbohydrate Research* **1982**, *108*, 1–11.
15. P. G. de Gennes *Scaling Concepts in Polymer Physics*; Cornell University Press: Itacha, New York, 1979.
16. A. M. Hecht, F. Horkay, P. Schleger, E. Geissler, *Macromolecules* **2002**, *35*, 8552–8555.
17. E. Geissler, F. Horkay, A. M. Hecht, C. Rochas, P. Lindner, C. Bourgaux, G. Courrazze, *Polymer* **1997**, *38*, 15–20.
18. F. Horkay, A. M. Hecht, E. Geissler, *Macromolecules* **1998**, *31*, 8851–8856.
19. I. Dogsa, M. Kriechbaum, D. Stopar, P. Laggner, *Biophys. J.* **2005**, *89*, 2711–2720.
20. I. Dogsa, M. Tomšič, J. Orehek, E. Benigar, A. Jamnik, D. Stopar, *Carbohydr. Polym.* **2014**, *111*, 492–504.
21. I. Dogsa, J. Štrancar, P. Laggner, D. Stopar, *Polymer* **2008**, *49*, 1398–1406.
22. O. Kratky, H. Stabinger, *Colloid Polym. Sci.* **1984**, *262*, 345–360.
23. D. Orthaber, A. Bergmann, O. Glatter, *J. Appl. Crystallogr.* **2000**, *33*, 218–225.
24. P. Debye, A. M. Bueche, *J. Chem. Phys.* **1948**, *16*, 573.
25. A. M. Hecht, F. Horkay, S. Mallam, E. Geissler, *Macromolecules* **1992**, *25*, 6915–6920.
26. M. Robitzer, L. David, C. Rochas, F. Di Renzo, F. Quignard, *Langmuir* **2008**, *24*, 12547–12552.
27. E. Shtykova, A. Dembo, E. Makhaeva, A. Khokhlov, G. Evmenenko, H. Reynaers, *Langmuir* **2000**, *16*, 5284–5288.
28. M. Gawronski, G. Aguirre, H. Conrad, T. Springer, K.-P. Stahmann, *Macromolecules* **1996**, *29*, 1516–1520.
29. H. Yamakawa, M. Fujii, *Macromolecules* **1974**, *7*, 128–135.

Povzetek

Polisaharid levan je homopolimer fruktoze. Levan je pomembna sestavina rastlin, kvasovk, gliv in nekaterih bakterijskih biofilmov. V tem delu poročamo o strukturnih značilnostih vodnih raztopin bakterijskih levanov z uporabo ozkokotnega rentgenskega sipanja in svetlobne mikroskopije. Poleg komercialno dostopnih levanov bakterij *Zymomonas mobilis* in *Erwinia herbicola*, smo izolirali, očistili in raziskovali tudi levan iz biofilma bakterije *Bacillus subtilis*. Rezultate ozkokotnega sipanja rentgenskih žarkov smo analizirali z modelom biserne verižice, ki je razkril kvalitativne razlike v strukturi molekul treh levanov. Molekule polimera si lahko predstavljamo in jih modeliramo kot delno fleksibilne verige, katerih konformacije so odvisne od intra- in intermolekularnih interakcij. Slednje so vzrok za različne suprastrukture, ki se tvorijo v sistemu na večjih velikostnih skalah. S povečevanjem koncentracije levana so postale strukture bolj kompaktne, kar smo opazili tako na nanoskali, kot tudi na mikroskali. Najbolj homogeno porazdeljene strukture glede na lokalno polimerno gostoto smo opazili pri levanu bakterije *B. subtilis*.